CHALMERS

Gravitational Instability of Two-Component Galactic Discs

Master of Science Thesis

NIKLAS FALSTAD

Supervisor: Alessandro Romeo

Department of Earth and Space Sciences
CHALMERS UNIVERSITY OF TECHNOLOGY
Gothenburg, Sweden, June 2012

Master's Thesis

Gravitational Instability of Two-Component Galactic Discs

NIKLAS FALSTAD
Supervisor: Alessandro Romeo

Department of Earth and Space Sciences
CHALMERS UNIVERSITY OF TECHNOLOGY
Gothenburg, Sweden

June 2012

Gravitational Instability of Two-Component Galactic Discs
NIKLAS FALSTAD

Department of Earth and Space Sciences
Chalmers University of Technology
SE-412 96 Gothenburg, Sweden
+46 31-772 1000

Onsala Space Observatory
SE-439 92 Onsala, Sweden
+46 31-772 5500

Abstract

The gravitational instability of galactic discs has been investigated for over 50 years, and several stability criteria have been proposed. A common approach is to consider a two-component disc of stars and gas, where both components are treated as fluids. A more realistic, but mathematically more complex, approach is to treat the stellar component as collisionless, using kinetic theory. In recent years, sensitive and high-resolution observations of nearby galaxies have provided data of unprecedented value. It is then important to assess the accuracy of those stability criteria when used for analysing such data. We therefore perform a rigorous comparative analysis, using a full set of stability diagnostics, of stability criteria based on the two approaches mentioned above. We find that the fluid-fluid stability criterion has almost the same accuracy as the kinetic-fluid criterion. We also find that, except in a small region of the parameter plane, the fluid-fluid approximation can be reliably used for finding the wavenumber at which the disc is most unstable. Under certain conditions, the contributions of stars and gas to the gravitational instability of the disc can decouple. We find that these conditions only change slightly when using the fluid-fluid approximation.

Acknowledgements

I would like to thank my supervisor Alessandro Romeo for suggesting this thesis topic and for offering help and guidance throughout the course of the work. It has been a pleasure to work with him.

Furthermore, I want to thank the referee, Hans Nordman, for valuable input that helped to improve the thesis.

I also want to thank the people at the Onsala Space Observatory for providing an inspiring environment to work in. Even though I only spent one day a week at the facility, it is where most of this work has been done.

Finally, all my love and thanks to Lina, who is always there for me.

Niklas Falstad
Gothenburg, June 2012

Contents

1

Introduction

Gravitational instabilities in galactic discs were studied already in the 1960's by Safronov (1960) and Toomre (1964), who considered one-component discs of stars or gas. The importance of considering discs consisting of both stars and cold interstellar gas was soon realized by Lin & Shu (1966), who were the first to use a two-component disc model. The threshold for such instabilities is an important stability diagnostic since it seems to be associated to the onset of galactic scale star formation (Kennicutt, 1989; Elmegreen, 1999).

Recently, nearby galaxies have been observed with high resolution and sensitivity in several surveys: The HI Nearby Galaxy Survey (THINGS) in which the 21-cm line of neutral hydrogen was observed (Walter et al., 2008), the Galaxy Evolution Explorer (GALEX) Nearby Galaxies Survey in which observations were made in the UV (Gil de Paz et al., 2007), the Spitzer Infrared Nearby Galaxies Survey (SINGS) in which observations were made in the IR (Kennicutt et al., 2003) and the HERA CO-Line Extragalactic Survey (HERACLES) in which CO line emission was observed (Leroy et al., 2009). Using data from such surveys one can, for example, study the rate of star formation (Leroy et al., 2008), a process in which gravitational instabilities play an important part (McKee & Ostriker, 2007; Elmegreen, 1999).

At high redshifts, observations have revealed that galaxies are richer in gas than those in the local universe (Daddi et al., 2008, 2010; Tacconi et al., 2008, 2010). These galaxies are also often dominated by kpc-sized star-forming clumps (e.g. Cowie et al., 1995; Elmegreen et al., 2004; Elmegreen & Elmegreen, 2005; Förster Schreiber et al., 2009). Observations indicate that these clumps and the discs where they reside are subject to gravitational instabilities (Genzel et al., 2011). With the construction of observatories like ALMA, it will soon be possible to observe these high-redshift galaxies at higher resolutions.

As present and future observations can provide us with data of unprecedented value, it is important to assess the accuracy of the approximations used in analysing such data. In the case of gravitational instabilities, a common approximation is to regard the galactic disc as made of two components, and to treat both gas and stars as fluids (Jog & Solomon, 1984; Bertin & Romeo, 1988; Elmegreen, 1995; Jog, 1996; Rafikov, 2001). In this thesis we will compare instability criteria based on this approximation with a more realistic criterion that treats stars as a collisionless component (Rafikov, 2001). In Chap. 2, we will overview the gravitational instability of galactic discs. A rigorous comparative analysis will then be carried out in Chap. 3 using a full set of stability diagnostics. We will also compare a simpler approximation, introduced by Romeo & Wiegert (2011), with the criterion based on the kinetic-fluid approach. The main conclusions that can be drawn from the analysis are then summarized in Chap. 4.

2

Gravitational instability of galactic discs: overview of previous work

Real galaxies are complex systems consisting of multiple components of stars and gas. In Sect. 2.1, we discuss the stability of a disc consisting of only one such component, either a gaseous or a stellar one. To account for the fact that the gas behaves like a fluid while the stellar populations are non-collisional, two different approaches to this one-component case are used. In Sect. 2.2, the discussion is expanded to include two components, studying the results of combining the two approaches from the one-component case.

2.1 One-component case

In both approaches, the response of a one-component axisymmetric disc is studied when it is subjected to perturbations in its density distribution. An important result of this study is the dispersion relation. This is an equation that relates the angular frequency, ω, of the perturbation to its wavenumber, k. The wavenumber is in its turn related to the wavelength like $k = 2\pi/\lambda$.

For the derivation of the dispersion relations, as well as a discussion of the various approximations used, see Binney & Tremaine (2008).

2.1.1 Fluid approach

In a gaseous disc, the behavior of the system is determined by both the short-range interparticle forces and the long-range force of gravity. Since gas is dominated by collisions, the disc can be described as a fluid using Euler's equation and the continuity equation, complemented by a polytropic equation of state and Poisson's equation.

These equations can then be used to find the dispersion relation for the gaseous disc:

$$\omega^2 = \kappa^2 - 2\pi G\Sigma|k| + \sigma_{\mathrm{g}}^2 k^2, \tag{2.1}$$

where ω is the angular frequency and k is the wavenumber of the density wave, while κ is the epicyclic frequency, σ_g is the sound speed and Σ is the surface density in the unperturbed disc.

As the density perturbation is proportional to $\exp(-i\omega t)$, the stability of the disc is determined by the sign of the left-hand side of this dispersion relation. If it is positive, ω will be real, the perturbation will oscillate with frequency ω and the disc will be stable. If, on the other hand, the left-hand side is negative, ω will be imaginary and the perturbation will grow exponentially, rendering the disc unstable.

In the light of the above discussion on the condition of stability, the effect of the three terms on the right-hand side of Eq. (2.1) on the disc can be understood. The first term, κ^2, which is related to the rotation, is always positive and tends to stabilize the disc. The second term, $-2\pi G\Sigma|k|$, is related to the self-gravity and it is always negative, having a destabilizing effect. The last term is due to the pressure and is again always positive, working to stabilize the disc.

Now, for the disc to always be stable, ω^2 has to be greater than zero for all wavenumbers. Inserting this condition into the dispersion relation (2.1) gives the following condition for stability:

$$Q_{\mathrm{g}} \equiv \frac{\kappa\sigma_{\mathrm{g}}}{\pi G\Sigma} > 1. \tag{2.2}$$

This is known as Toomre's stability criterion[1].

2.1.2 Kinetic approach

In the stellar case, the fluid equations cannot in principle be used to describe the disc since the ensamble of stars in a galactic disc is collisionless. Instead, a kinetic approach to the problem has to be used, describing the disc with a distribution function f, where $f(\mathbf{x},\mathbf{v},t)\mathrm{d}^3\mathbf{x}\mathrm{d}^3\mathbf{v}$ describes the probability to find a randomly chosen star in the phase-space volume $\mathrm{d}^3\mathbf{x}\mathrm{d}^3\mathbf{v}$ around $\mathbf{x}$ and $\mathbf{v}$ at time t. For the unperturbed disc, a Schwarzschild distribution function is assumed. The time evolution of the distribution function is described by the collisionless Boltzmann equation[2].

Together with Poisson's equation, these equations can be used to calculate the stellar dispersion relation

$$\omega^2 = \kappa^2 - 2\pi G\Sigma|k|\mathcal{F}. \tag{2.3}$$

The reduction factor $\mathcal{F}$ in the dispersion relation is given by

$$\mathcal{F}\left(\frac{\omega}{\kappa},\frac{\sigma_\star^2 k^2}{\kappa^2}\right) = \mathcal{F}(s,\chi) = \frac{2}{\chi}(1-s^2)e^{-\chi}\sum_{n=1}^{\infty}\frac{I_n(\chi)}{1-s^2/n^2}, \tag{2.4}$$

where $\sigma_\star$ is the radial velocity dispersion and $I_n(\chi)$ is a modified Bessel function.

Like in the fluid approach, a stability criterion for the stellar disc can be formulated:

$$Q_{\star\mathrm{c}} \equiv \frac{\kappa\sigma_\star}{3.36G\Sigma} > 1. \tag{2.5}$$

This Toomre criterion for the stellar disc is almost identical to the one for the fluid disc (see fig 6.13 of Binney & Tremaine, 2008). The two differences are that π is changed to 3.36 and that the sound speed is replaced by the radial velocity dispersion.

Note, however, that for mathematical convenience the fluid approach is often used when analysing stellar discs.

[1] Sometimes the Safronov-Toomre stability criterion.

[2] Also called the Vlasov equation.

2.2 Two-component case

With the simpler one-component case studied in Sect. 2.1, it is now time to discuss the case of two components coexisting in the same galactic disc, coupled through their combined gravitational potential. The disc can then be modeled either as consisting of two fluid components or, in the more realistic but also more mathematically complex way, as one kinetic and one fluid component. The problem of gravitational instability in such discs has been studied by several authors.

The first of the cases, the fluid-fluid approximation, has been studied by Jog & Solomon (1984) [who where also the first to find its dispersion relation], Bertin & Romeo (1988), Elmegreen (1995) and Jog (1996). The kinetic-fluid case along with its dispersion relation was studied already by Lin & Shu (1966) [See also Lin et al. (1969)].

Relatively recently, Rafikov (2001) presented a dispersion relation for a disc composed of gas and multiple stellar components:

$$2\pi Gk\frac{\Sigma_{\mathrm{g}}}{\kappa^2+k^2\sigma_{\mathrm{g}}^2-\omega^2}+2\pi Gk\sum_{j=1}^{n_{\mathrm{s}}}\frac{\Sigma_j\mathcal{F}_j}{\kappa^2-\omega^2}=1, \tag{2.6}$$

where Σ_{g} and Σ_{j} are the surface densities of the gaseous and stellar components and $\mathcal{F}_j$ are the reduction factors, as in Eq. (2.4), for the different stellar components.

Apart from the dispersion relation, Rafikov also presented instability conditions for the two-component disc in the fluid-fluid and the kinetic-fluid case. To write these conditions in a simple form, the following dimensionless quantities can be used:

$$Q_\star=\frac{\kappa\sigma_\star}{\pi G\Sigma_\star}, \qquad q=\frac{Q_{\mathrm{g}}}{Q_\star} \tag{2.7}$$

$$K=\frac{k\sigma_\star}{\kappa}, \qquad s=\frac{\sigma_{\mathrm{g}}}{\sigma_\star}. \tag{2.8}$$

Note that $Q_\star$ is different from Toomre's stability parameter for stellar systems by a factor of 1.07. Romeo & Wiegert (2011) used data of nearby galaxies from Leroy et al. (2008), and found that they fall within the ranges $0.01 \lesssim s \lesssim 1$ and $0.1 \lesssim q \lesssim 10$. In the solar neighbourhood, the values are found to be $s\approx 0.2$ and $q\approx 0.6$ (see Binney & Tremaine, 2008, p. 497).

Written using these quantities, the instability conditions are

$$\frac{2}{Q_\star}\frac{K}{1+K^2}+\frac{2}{Q_\star}\frac{1}{q}\frac{Ks}{1+K^2s^2}>1, \tag{2.9}$$

in the fluid-fluid case and

$$\frac{2}{Q_\star K}[1-e^{-K^2}I_0(K^2)]+\frac{2}{Q_\star}\frac{1}{q}\frac{Ks}{1+K^2s^2}>1, \tag{2.10}$$

in the kinetic-fluid case. Due to the fact that $Q_\star$ is different from Toomre's stability parameter for stellar systems, a purely stellar disc is gravitationally unstable for $Q_\star < 1.07$ in this parametrization. If it is preferred to use the stellar Toomre parameter, this can be accomplished by a simple reparametrization.

3

Comparative stability analysis of two-component discs

In this chapter, we use Eqs (2.9) and (2.10) to study some different stability diagnostics in the s-q plane. In Sect. 3.1, we evaluate the left-hand sides of these conditions as functions of K, the dimensionless wavenumber, for different values of the parameters s, q and $Q_\star$. The regions where the contributions of stars and gas to the gravitational instability decouple are then explored in Sect. 3.2. In Sect. 3.3, we study the threshold for gravitational stability along with the error made when using the fluid-fluid approximation for an effective stability parameter. We also make a comparison with an even simpler approximation by Romeo & Wiegert (2011) here. In Sect. 3.4, we study the most unstable wavenumber, along with the error made when using the fluid-fluid approximation, or a simpler approximation, for this wavenumber. Finally, in Sect. 3.5, we compare Rafikov's criteria to the works of Lin & Shu (1966), Bertin & Romeo (1988), Elmegreen (1995) and Jog (1996).

3.1 Stability curves

To understand how the parameters s, q and $Q_\star$ affect the stability of the disc, we first study the left-hand sides of the instability conditions in Eqs (2.9) and (2.10) as functions of K. As they tell us for which wavenumbers the disc is stable, the resulting curves are referred to as the stability curves. Keep in mind that wherever the stability curve has a value greater than one, the disc is gravitationally unstable against perturbations with the corresponding wavenumber.

In both of Eqs (2.9) and (2.10), the first and the second term on the left-hand side correspond to the stellar and the gaseous component, respectively. When studied individually as functions of K, the stellar term forms a curve peaking at a low wavenumber while the curve of the gaseous term peaks at a higher, s-dependant, wavenumber. The total stability curve is then a superposition of these two curves.

The first parameter to be studied, s, affects where the gaseous component has its maximum, thus deciding how close together the two peaks are. For sufficiently high s the two peaks join to form a single maximum, and when s becomes equal to one the gas and stars act like a single component. We illustrate this in Fig. 3.1, where s is varied from 0.1 to 1.0.

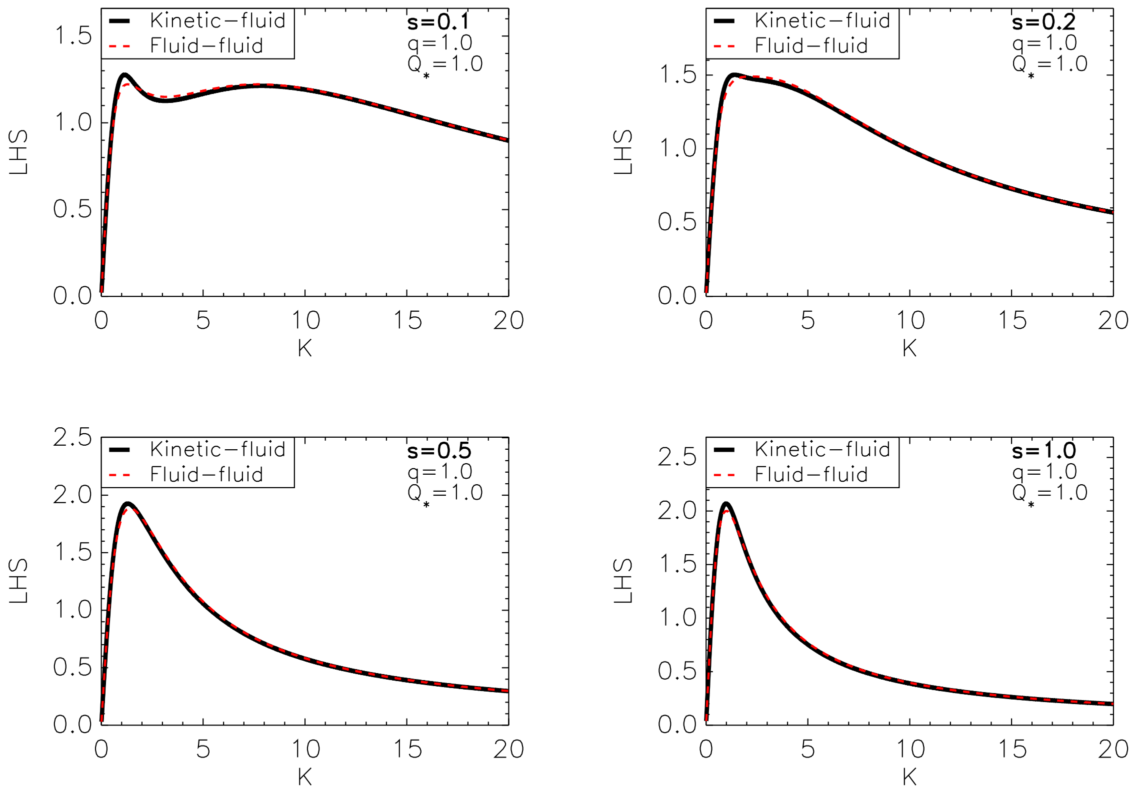

Figure 3.1: Illustration of how the stability curves vary with changing s, note how the peaks move closer and eventually join together in a single peak for the higher values of s.

The second parameter, q, affects the height of the gaseous peak relative to the stellar one, a higher q meaning a more dominant stellar component. This is illustrated in Fig. 3.2. Note that even with the same values of s and $Q_\star$ as in the first curve of Fig. 3.1, the total curve can exhibit only one peak if one of the components is sufficiently dominant.

The final parameter that we vary is $Q_\star$, which only affects the scaling of the curves. As is seen in Fig. 3.3, the shapes of the curves are identical, but the scaling of the left-hand side axis changes with changing $Q_\star$.

Something that is evident in all of Figs 3.1-3.3 is that the curves describing the fluid-fluid approximation are not very different from the ones describing the more realistic kinetic-fluid case. The small difference that does show is mainly located around the stellar peak. This is due to the fact that the stellar term of the kinetic case is slightly more peaked, reaching a higher maximum value, than the one of the fluid approximation. That is also why the error is most noticeable around the stellar peak.

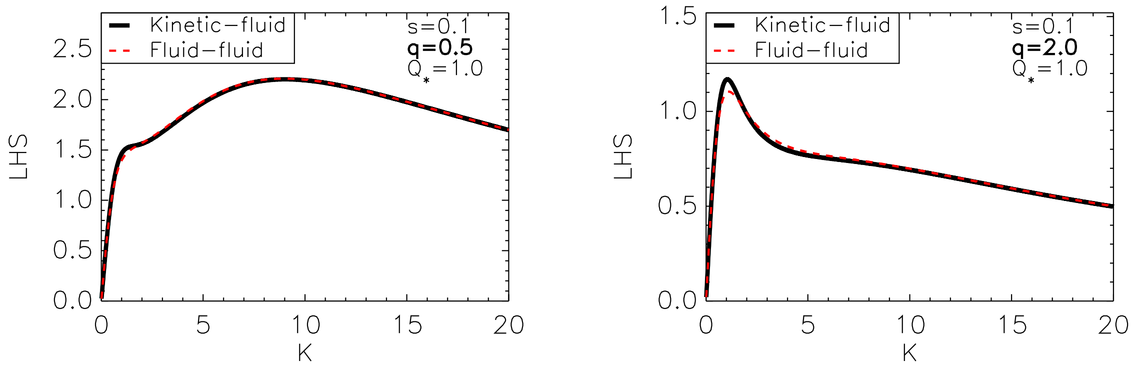

Figure 3.2: Illustration of how the stability curves vary with changing q. Compare also with the first curve of Fig. 3.1 where q is equal to one.

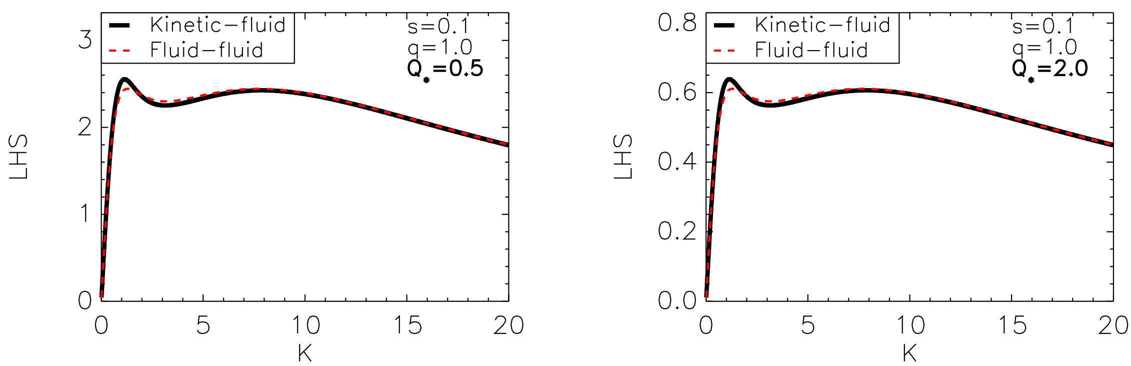

Figure 3.3: Illustration of how the stability curves vary with $Q_\star$. Note that it is only the scaling of the left-hand side axis that changes.

3.2 The condition for star-gas decoupling

We saw in Sect. 3.1 that depending on the parameters, the stability curve can have either one or two distinct peaks. When the curve exhibits only one peak, the maximum corresponds to a well defined wavenumber at which the disc will first encounter instability. When, on the other hand, the curve has two distinct peaks, there are two wavenumbers at which the instability can first set in, depending on which peak is the highest.

The region in the s-q plane where the stability curve exhibits two peaks is the same as the two-phase region investigated by Bertin & Romeo (1988). In the left panel of Fig. 3.4 we outline this region for both the kinetic-fluid and the fluid-fluid case. The right panel shows the same thing with the kinetic-fluid case parametrized using $Q_{\star c} = \kappa\sigma_\star/3.36G\Sigma_\star$ as discussed at the end of Sect. 2.2. Note that in both panels, the two-phase region expands in the kinetic-fluid case, but also that it is displaced downwards when using Rafikov's original parametrization.

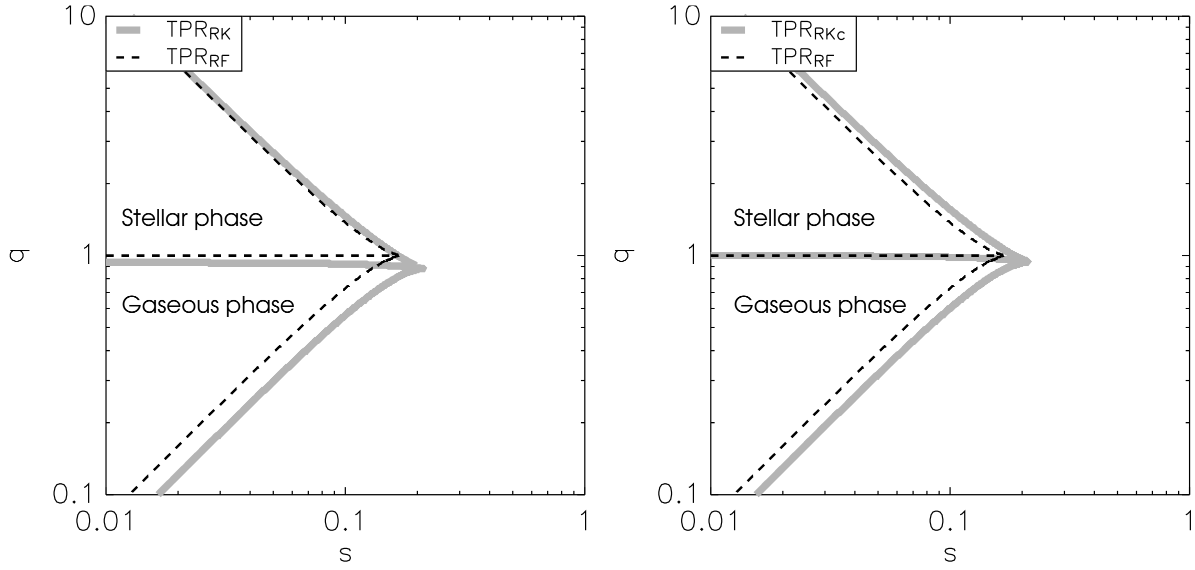

Figure 3.4: The two-phase regions for the fluid-fluid (RF) approximation and the more realistic kinetic-fluid (RK) treatment. To the left, the kinetic-fluid case is treated in the same way as by Rafikov. To the right, the stability condition for this case has been reparametrized to use the Toomre parameter for stellar discs.

For each of the two-phase regions in Fig. 3.4 there is a special important point in the parameter plane, by Bertin & Romeo (1988) called the triple point. This is the point where the boundaries of the two-phase region intersect with the transition line between the stellar and gaseous phases within the region. The nature of the triple point leads to a single very flat maximum of the stability curve for the parameters in question.

We have listed the coordinates of the triple point in the parameter plane in Table 3.1, together with the stability threshold and the least stable wavenumber at these coordinates. The last two quantities are examples of important diagnostics which are discussed further in Sects 3.3 and 3.4.

Table 3.1: Location of the triple point in the s-q plane and the stability threshold $\overline{Q}$ and least stable wavenumber $K_{\max}$ at these coordinates.

Case	s_0	q_0	$\overline{Q}_0$	$K_{\max 0}$
Fluid-fluid	0.17	1.00	1.4	1.9
Kinetic-fluid	0.21	0.88	1.6	2.4
Kinetic-fluid(corr)	0.21	0.94	1.5	2.5

3.3 The stability threshold

From the instability conditions in Eqs (2.9) and (2.10) we see that the disc is gravitationally stable at all wavenumbers if the value of the stability curve is always less than one. Thus, we can define effective stability parameters which have values higher or lower than one for stable or unstable discs, respectively, like

$$\frac{1}{\overline{Q}_{\mathrm{RF}}} = \max_K \left(\frac{2}{Q_\star} \frac{K}{1+K^2} + \frac{2}{Q_\star} \frac{1}{q} \frac{Ks}{1+K^2 s^2} \right), \tag{3.1}$$

in the fluid-fluid approximation and

$$\frac{1}{\overline{Q}_{\mathrm{RK}}} = \max_K \left(\frac{2}{Q_\star K} \left[1 - e^{-K^2} I_0(K^2) \right] + \frac{2}{Q_\star} \frac{1}{q} \frac{Ks}{1+K^2 s^2} \right), \tag{3.2}$$

in the kinetic-fluid case.

We can rewrite these effective stability parameters as

$$Q_{\mathrm{eff}} = \frac{Q_\star}{\overline{Q}} \tag{3.3}$$

where $\overline{Q}$ is the stability threshold above which the disc is stable and Q_{eff} is the effective stability parameter. We show the contour lines of these stability thresholds in the fluid-fluid approximation and the kinetic-fluid case in the left panel of Fig. 3.5. In the right panel, we have reparametrized the kinetic-fluid case as described in the end of Sect. 2.2. For the three first contours in both panels, the transition from the gaseous to the stellar phase within the two-phase region is apparent.

As the stability threshold varies slowly in the upper part of the s-q plane, even a small difference will show up as a large displacement of the contour lines. In the left panel of Fig. 3.5, this leads to large discrepancies between the contours of the approximation and the kinetic-fluid case, even though the quantitative differences are small.

A better way to visualize the quantitative accuracy is to use the relative error of the two cases, $(Q_{\mathrm{RF}} - Q_{\mathrm{RK}})/Q_{\mathrm{RK}}$. In this case it is equal to the relative error of the inverse stability threshold $(1/\overline{Q}_{\mathrm{RF}} - 1/\overline{Q}_{\mathrm{RK}}) \cdot \overline{Q}_{\mathrm{RK}}$. This is displayed in Fig. 3.6 where we can see that the maximum error actually is less than 7%. As usual, the right panel shows the same thing but with a reparametrization. From this figure it is evident that the fluid-fluid approximation fits better when we compare it to the reparametrized kinetic-fluid case. Not only is the absolute maximum error less, the larger errors are also confined to a smaller region in the s-q plane. Note also that the error when we do the reparametrization is always negative, while the error when we use original parametrization changes sign in a small region around the triple-point.

From the above analysis, it is evident that the fluid-fluid approximation works well for most values of the parameters s and q, especially when compared to the reparametrized kinetic-fluid case. An even simpler, approximate, form of the effective stability parameter in the fluid-fluid case was suggested by Romeo & Wiegert (2011). They also showed that the relative error when using their approximation instead of the real fluid-fluid approximation is always less than 9%.

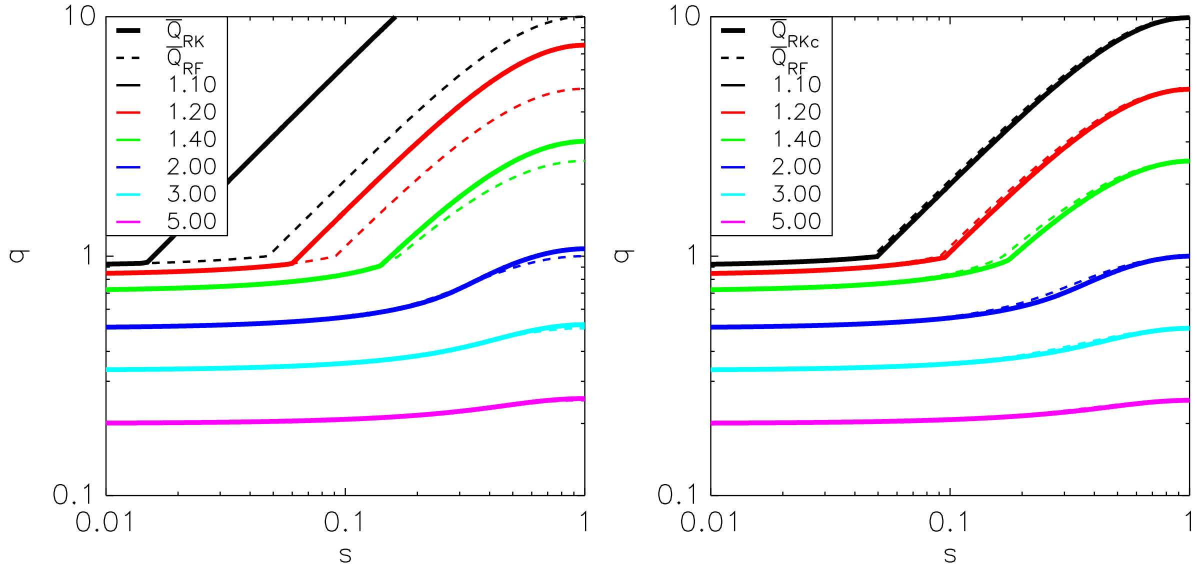

Figure 3.5: Contour lines of the stability thresholds $\overline{Q}$ in the fluid-fluid approximation and the kinetic-fluid case. To the right, the kinetic-fluid case is parametrized using the stellar Toomre parameter. Note the abrupt change in slope as the lines pass the transition line between the gaseous and stellar phases within the two-phase region.

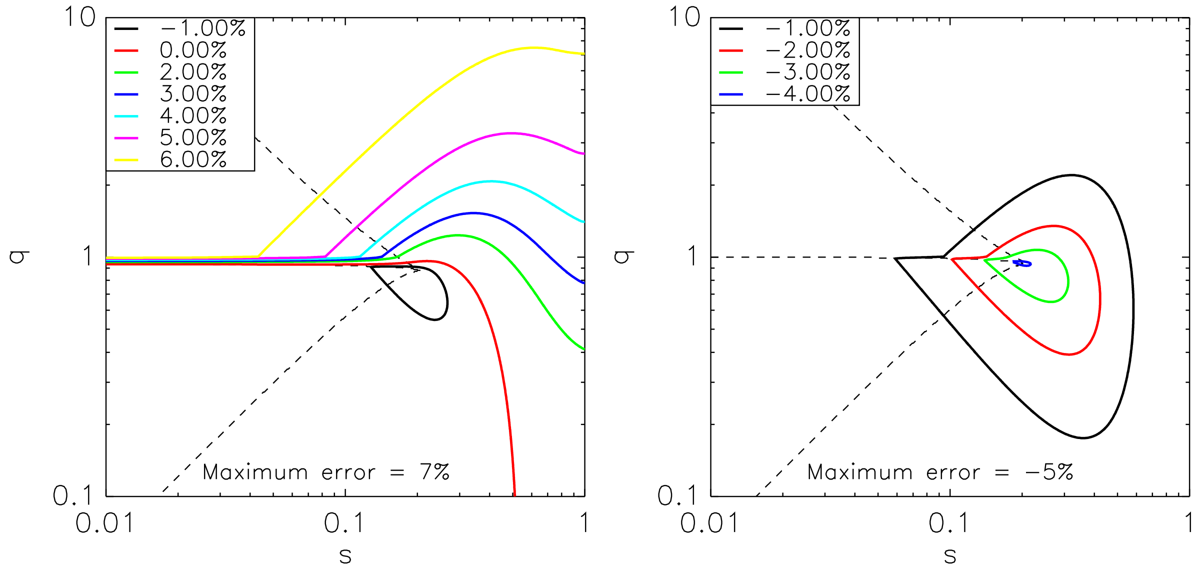

Figure 3.6: Contour lines of the relative error $(Q_{\mathrm{RF}} - Q_{\mathrm{RK}})/Q_{\mathrm{RK}}$, in the right panel the kinetic-fluid case is reparametrized as discussed in the end of Sect. 2.2. In both panels the image is superimposed on the two-phase region of the kinetic-fluid case.

The Romeo-Wiegert approximation is defined as follows:

$$\frac{1}{Q} = \begin{cases} \dfrac{W(s)}{Q_\star} + \dfrac{1}{Q_\star}\dfrac{1}{q} & \text{if } q \le 1\,, \\[2ex] \dfrac{1}{Q_\star} + \dfrac{W(s)}{Q_\star}\dfrac{1}{q} & \text{if } q \ge 1\,, \end{cases} \tag{3.4}$$

where $W(s)$ is defined as

$$W(s) = \frac{2s}{1+s^2}\,. \tag{3.5}$$

In Fig. 3.7, contour lines of the stability threshold calculated from this approximation are shown together with the ones of the kinetic-fluid case, both the original and the reparametrized one.

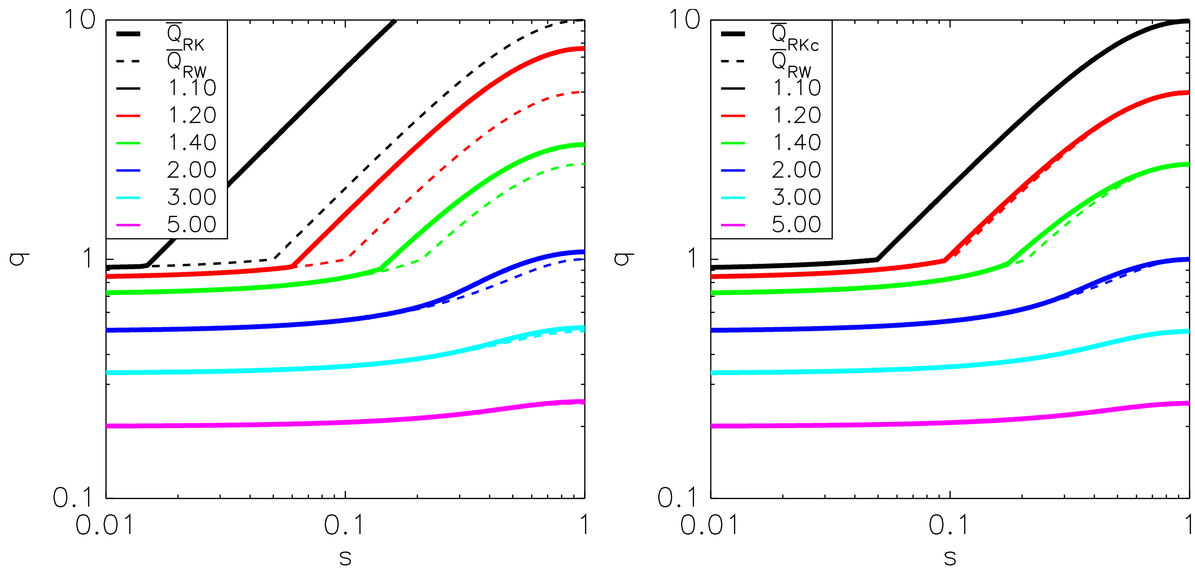

Figure 3.7: Contour lines of the stability thresholds $\overline{Q}$ in the Romeo-Wiegert approximation and the kinetic-fluid case. To the right, we have reparametrized the kinetic-fluid case as described in the end of Sect. 2.2.

The relative error of the Romeo-Wiegert approximation against the kinetic fluid case is shown in the left panel of Fig. 3.8. In the right panel, we show the same thing with the the kinetic-fluid case reparametrized. The maximum error when compared to the reparametrized case is actually smaller, 6% against 9%, than the one Romeo & Wiegert found when comparing with the fluid-fluid approximation.

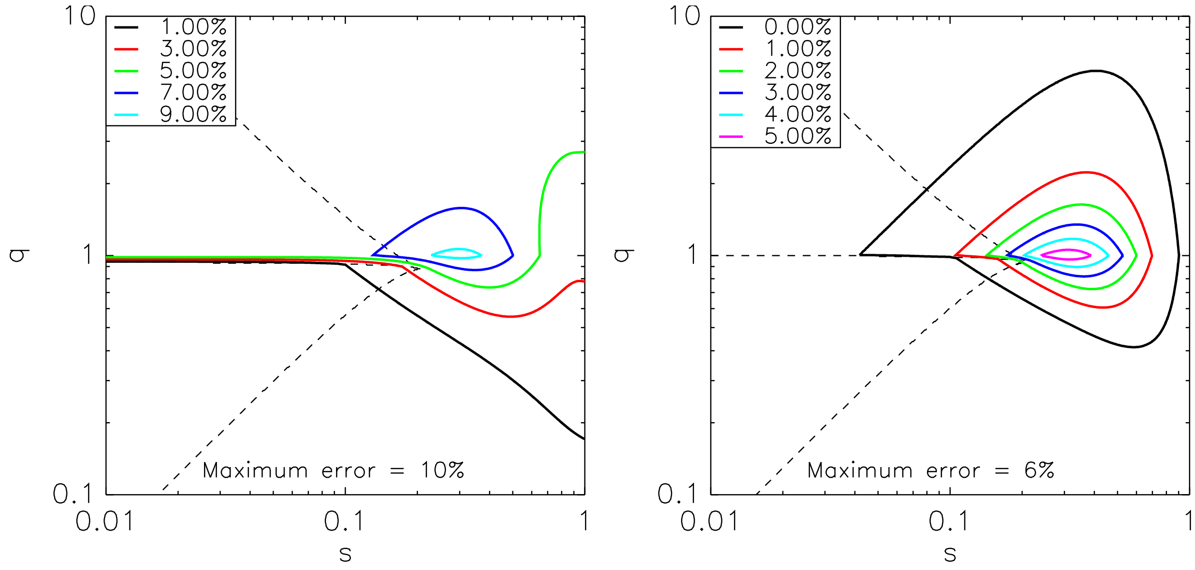

Figure 3.8: Contour lines of the relative error of the Romeo-Wiegert approximation against the kinetic-fluid case, in the right panel the latter is again reparametrized. In both panels the image is superimposed on the two-phase region of the kinetic-fluid case.

3.4 The most unstable wavenumber

Another important stability diagnostic is the most unstable wavenumber, the wavenumber at which $\omega^2(k)$ is at its minimum. At the stability threshold, this is the same as the wavenumber that maximizes the stability curve, $K_{\max}$. Contours of $K_{\max}$ in both the fluid-fluid approximation and the kinetic-fluid case are illustrated in Fig. 3.9. In the upper, star-dominated, region of the parameter plane $K_{\max}$ varies slowly, so even though the contours of the two cases are far away from each other, the quantitative error is not large.

The relative error $(K_{\max,\mathrm{RF}} - K_{\max,\mathrm{RK}})/K_{\max,\mathrm{RK}}$ of the least stable wavenumber in the fluid-fluid approximation is shown in Fig. 3.10. Here we see that the fluid-fluid approximation works reasonably well almost everywhere in the parameter plane, it only starts to deteriorate close to the triple-point. There is also a very tight region, surrounding the transition line inside the two-phase region, where the error in $K_{\max}$ is larger than 100%. This is because the phase change occurs at different q in the two cases [see Fig. 3.4], meaning that in this region the two cases are dominated by different components. In the fluid-fluid case the gaseous peak is the highest, while in the kinetic-fluid case the stellar peak, at a much lower wavenumber, is higher. With the reparametrization, the transition lines of the two cases are closer, making the region of large error much smaller.

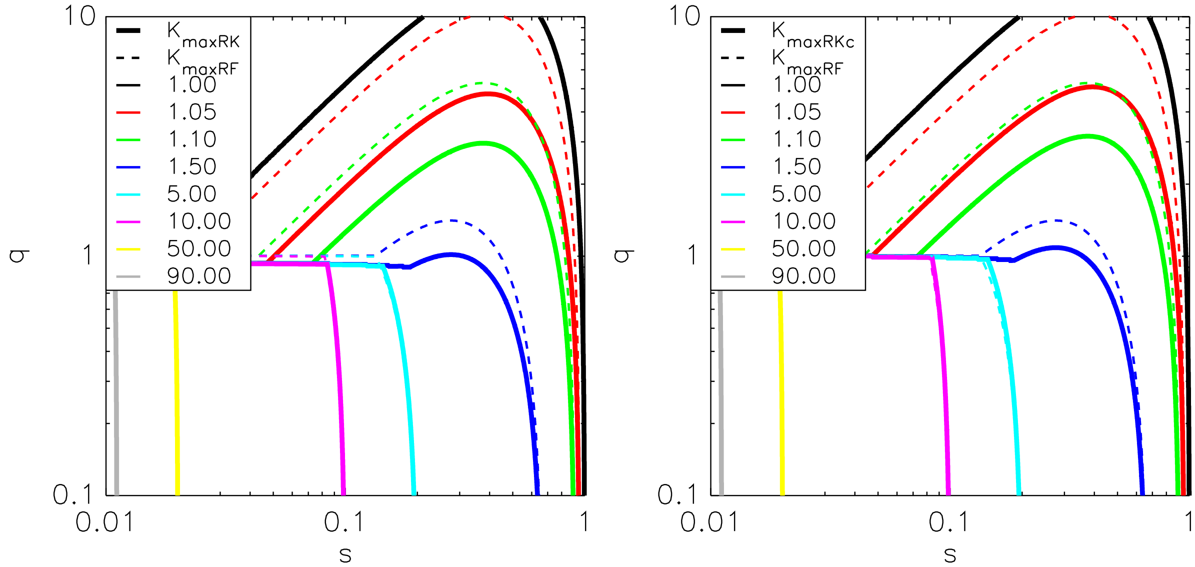

Figure 3.9: The least stable wavenumber at the stability threshold, both the fluid-fluid approximation and the kinetic-fluid case. To the right, we have applied the reparametrization of Sect. 2.2 to the kinetic-fluid case.

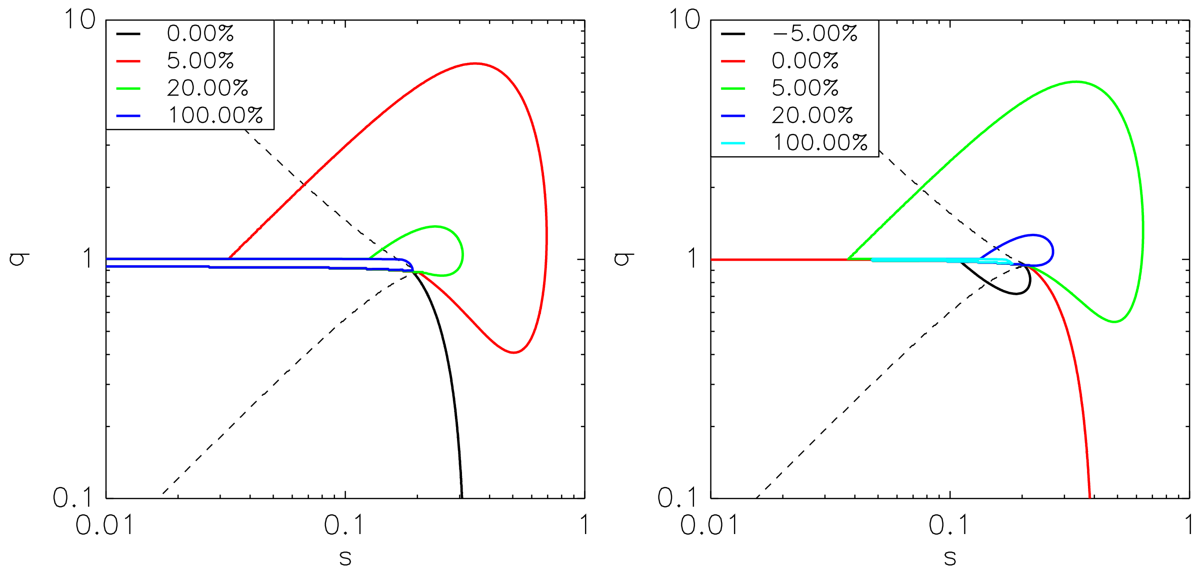

Figure 3.10: The relative error of $K_{\max}$ in the fluid-fluid approximation, note how the error goes above 100% around the transition line in the two-phase region. In the right panel, the kinetic-fluid case has been reparametrized as discussed in the end of Sect. 2.2. With this reparametrization, the region of very large error is much smaller.

The stability curves, i.e. the left-hand sides of Eqs (2.9) and (2.10), both consist of two terms, each with its own distinct maximum. Guided by this form, we can construct a simple approximation for $K_{\max}$ by using the wavenumber that maximizes the dominant term. If we take $q = 1$ to be the transition line between gas- and stellar domination, the approximation is:

$$K_{\max,\mathrm{app}} = \begin{cases} \dfrac{1}{s} & \text{if } q < 1\,, \\ \\ 1 & \text{if } q > 1\,. \end{cases} \tag{3.6}$$

The $K_{\max}$ from this approximation are shown, together with the ones from the kinetic-fluid treatment, in Fig. 3.11. Again, in the upper, star-dominated, region of the parameter plane $K_{\max}$ varies slowly and is always close to one. Setting $K_{\max,\mathrm{app}}$ to one in this region therefore produces no large quantitative errors, even though it cannot reproduce the qualitative behaviour of $K_{\max}$.

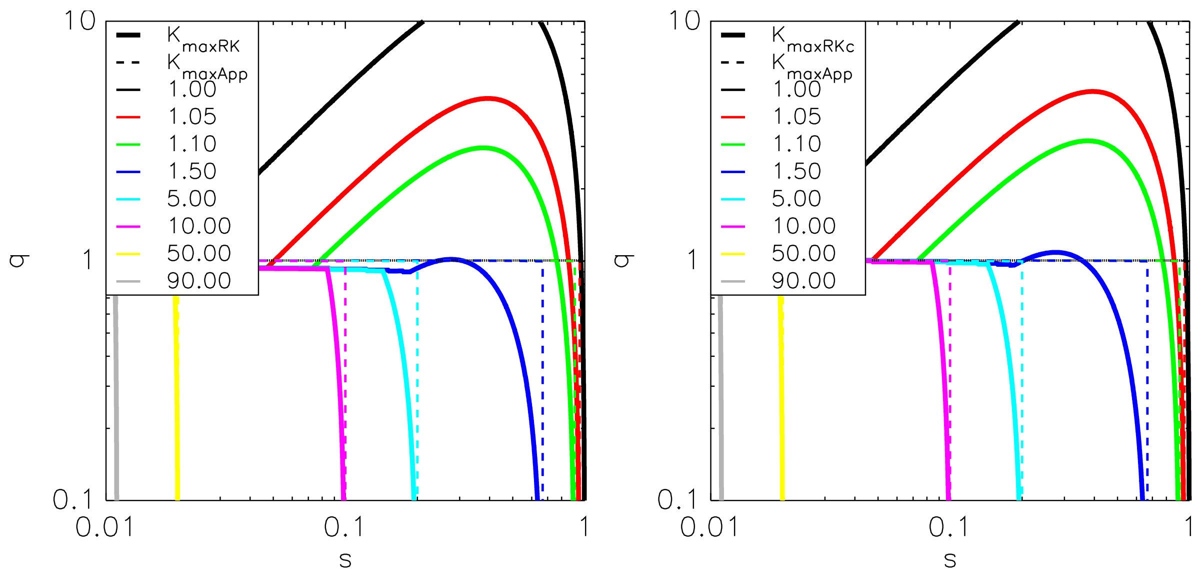

Figure 3.11: The approximation of $K_{\max}$ together with $K_{\max}$ from the kinetic-fluid case. To the right, the kinetic-fluid case is reparametrized as discussed at the end of Sect. 2.2. The only difference that comes out of this is a vertical displacement of the contours.

In Fig. 3.12 we show the relative error, $(K_{\max,\mathrm{app}} - K_{\max,\mathrm{RK}})/K_{\max,\mathrm{RK}}$, of the approximate $K_{\max}$. There we see that the approximation works fairly good everywhere except close to the triple-point. Like in the fluid-fluid approximation, there is again a tight region around the transition line in the two-phase region where the error is much larger than 100%. Because the real $K_{\max}$ is always in between the maxima of the two single components, the approximation is underestimating $K_{\max}$ for $q > 1$ and overestimating it for $q < 1$.

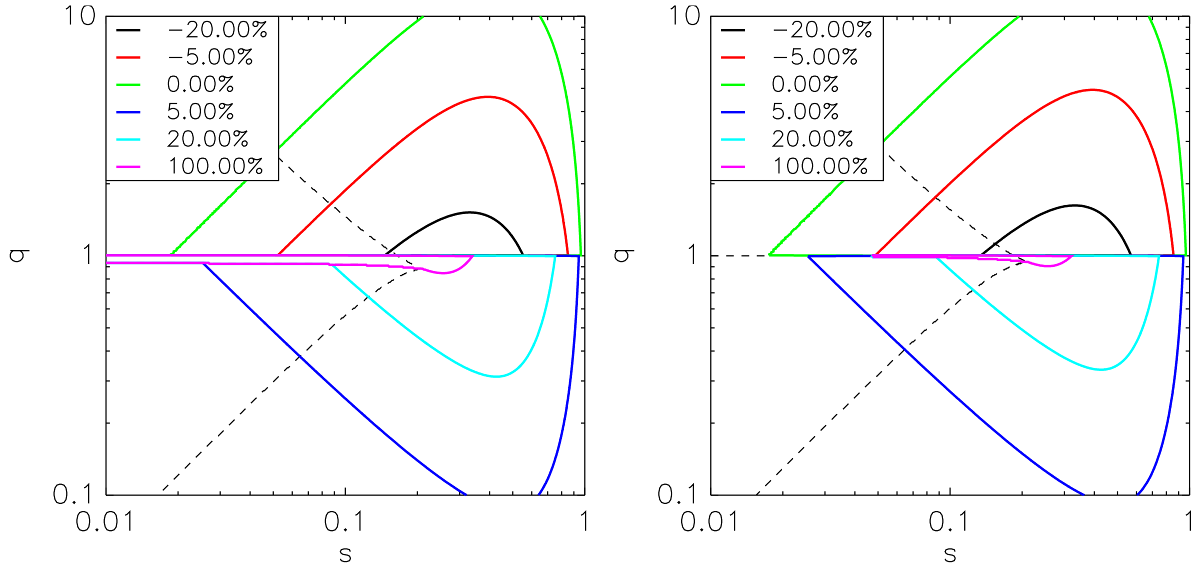

Figure 3.12: The relative error of $K_{\max}$ from the simple approximation in Eq. (3.6), note how the error again goes above 100% around the transition line in the two-phase region. To the right, we have applied the reparametrization of Sect. 2.2 to the kinetic-fluid case. Here the region of very large error is again much smaller.

Finally, if we use this approximation for $K_{\max}$ in Eq. (3.1) for the effective stability parameter, we obtain the Romeo-Wiegert approximation of Eq. (3.4) in a new way. Comparing Figs 3.12 and 3.8 we see that even though the error of the approximate $K_{\max}$ can be very large, the error in the effective stability parameter obtained using it never exceeds 10%.

3.5 Comparison between various stability criteria

Over the years, a variety of stability criteria has been presented by different authors. In this section, we compare the stability thresholds found in section 3.3 with those found by analysing the works of Lin & Shu (1966) in the kinetic-fluid case, and Bertin & Romeo (1988), Elmegreen (1995) and Jog (1996) in the fluid-fluid approximation.

Although these criteria all look different from each other, they are actually based on the same dispersion relation and should prove to be the same when compared. In the literature, there has been no such comparison between stability criteria so far, so we make it here.

In Sects 3.5.1-3.5.4 we compare the criteria in detail. This comparison is summarized in Fig. 3.13 where we see that, where they are defined, the stability thresholds agree with the ones of Rafikov from Sect. 3.3.

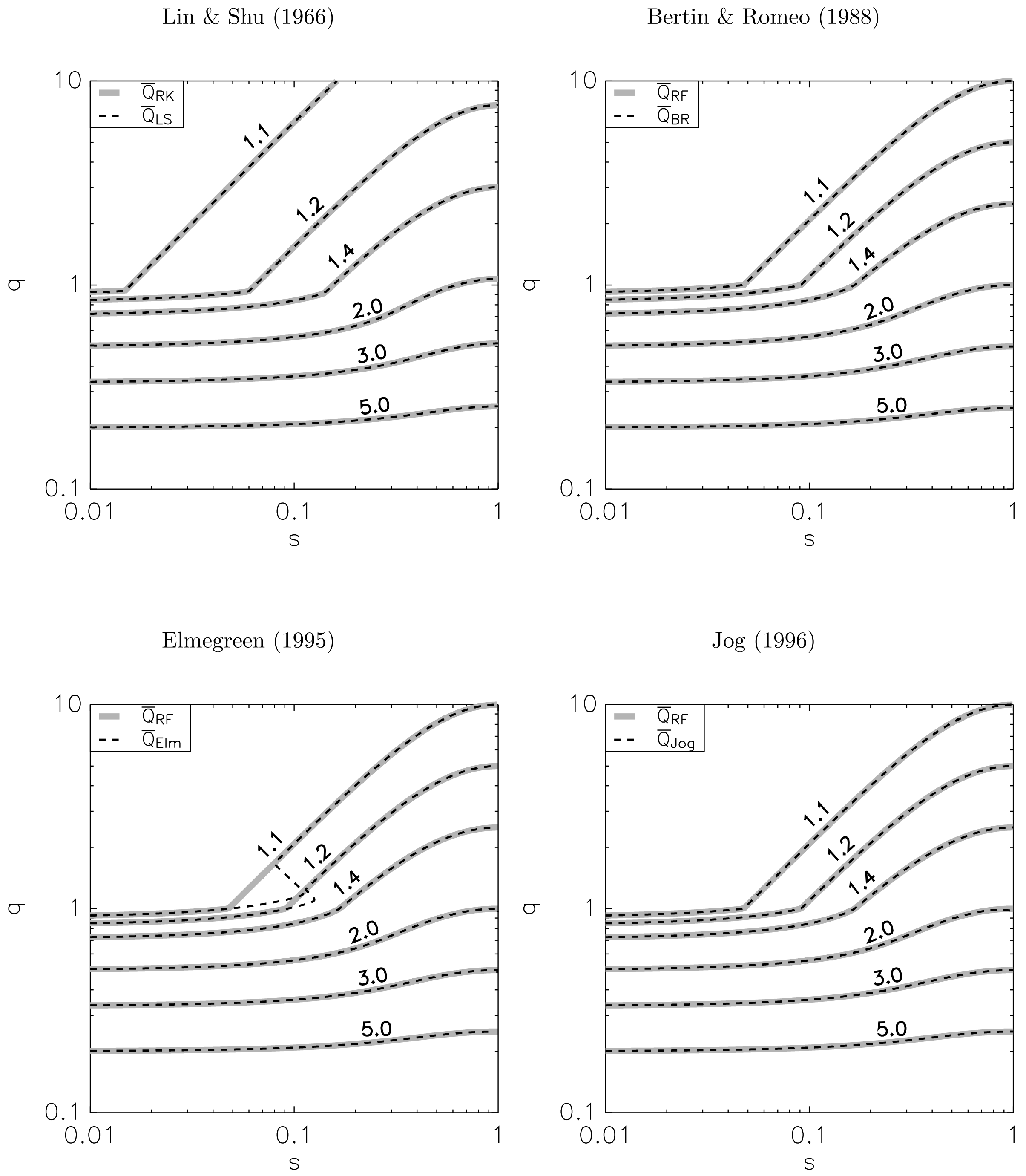

Figure 3.13: Contours of the stability thresholds discussed in Sects 3.5.1-3.5.4 vs. those of Rafikov (2001).

3.5.1 Lin & Shu (1966)

Lin & Shu (1966) found the dispersion relation in the kinetic-fluid case and wrote it like:

$$|k| = \frac{\kappa^2 - \omega^2}{2\pi G[\Sigma_\mathrm{g}\mathcal{F}_{\nu,\mathrm{g}}(x_\mathrm{g}) + \Sigma_\star\mathcal{F}_\nu(x)]}, \tag{3.7}$$

where $\nu = \omega/\kappa$, $x = k^2\sigma_\star^2/\kappa^2 (= K^2)$ and $x_\mathrm{g} = k^2\sigma_\mathrm{g}^2/\kappa^2 (= K^2 s^2)$. In parentheses, the quantities are expressed using our parameters as defined in Eqs (2.7) and (2.8). The reduction factor for the stars, $\mathcal{F}_\nu(x)$, is given by

$$\mathcal{F}_\nu(x) = \frac{1-\nu^2}{x}\left(1 - \frac{\nu\pi}{\sin\nu\pi}\cdot\frac{1}{2\pi}\int_{-\pi}^{\pi} e^{-x(1+\cos s)}\cos\nu s\,\mathrm{d}s\right). \tag{3.8}$$

The reduction factor for the gas is not a part of their original dispersion relation, but they state that it has to be included to get realistic results. As they don't supply it, we use the one of a later paper (Lin et al., 1969):

$$\mathcal{F}_{\nu,\mathrm{g}}(x_\mathrm{g}) = \frac{1}{1 + x_\mathrm{g}/(1-\nu^2)}. \tag{3.9}$$

When we combine Eqs (3.7)-(3.9), set $\omega^2 = 0$ and find the maximum value of $Q_\star$ which is able to satisfy the equation, we obtain the stability thresholds illustrated in the upper left panel of Fig. 3.13. There we see that these stability thresholds agree with the ones of Rafikov's kinetic-fluid case. Because of the integral that has to be evaluated every iteration, they are, however, slower to compute than the ones of Rafikov.

3.5.2 Bertin & Romeo (1988)

In their paper, Bertin & Romeo (1988) define a marginal stability curve in the ($\overline{\lambda}$,$Q_\star^2$)-plane as

$$\begin{aligned} MSC(\overline{\lambda}) = \left(\frac{2\overline{\lambda}}{\beta}\right)\cdot\Big[&(\alpha+\beta) - \overline{\lambda}(1+\beta) \\ &+ \sqrt{\overline{\lambda}^2(1-\beta)^2 - 2\overline{\lambda}(1-\beta)(\alpha-\beta) + (\alpha+\beta)^2}\Big], \end{aligned} \tag{3.10}$$

where $\alpha = \Sigma_\mathrm{g}/\Sigma_\star (= s/q)$, $\beta = \sigma_\mathrm{g}^2/\sigma_\star^2 (= s^2)$ and $\overline{\lambda}$ is a dimensionless wavelength. This marginal stability curve constitutes the border between stability and instability. Wherever the value of $Q_\star^2$ is above the curve, the disc is stable. To find the stability threshold, we maximize the curve and take the square root of the maximum value. The result of this process is shown in the upper right panel of Fig. 3.13, where we see that the stability thresholds are identical to the ones of Rafikov's fluid-fluid case.

3.5.3 Elmegreen (1995)

Elmegreen (1995) defines the effective stability parameter as

$$Q_{\rm Elm}^2 = \frac{Q_{\rm A}^2}{\mathcal{K}_{\rm min}[1+(1+\mathcal{C})^{1/2}] - \mathcal{K}_{\rm min}^2]} \tag{3.11}$$

where $Q_{\rm A}$ is given by

$$Q_{\rm A} = \frac{\kappa\sqrt{\sigma_\star^2+\sigma_{\rm g}^2}}{\sqrt{2}\pi G(\Sigma_\star+\Sigma_{\rm g})} \left(= Q_\star \frac{\sqrt{\frac{1}{2}(1+s^2)}}{1+\frac{s}{q}} \right), \tag{3.12}$$

and $\mathcal{C}$ is given by

$$\begin{aligned} \mathcal{C} = \frac{1}{4}\left(\frac{k(\sigma_\star^2-\sigma_{\rm g}^2)}{\pi G(\Sigma_\star+\Sigma_{\rm g})}\right)^2 - \frac{\Sigma_\star-\Sigma_{\rm g}}{\Sigma_\star+\Sigma_{\rm g}}\left(\frac{k(\sigma_\star^2-\sigma_{\rm g}^2)}{\pi G(\Sigma_\star+\Sigma_{\rm g})}\right) \\ \left(= \left(\mathcal{K}\frac{1-s^2}{1+s^2}\right)^2 - \frac{1-\frac{s}{q}}{1+\frac{s}{q}}\left(\mathcal{K}\frac{1-s^2}{1+s^2}\right)\right). \end{aligned} \tag{3.13}$$

The dimensionless wavenumber $\mathcal{K}$ is defined as

$$\mathcal{K} = \frac{k(\sigma_\star^2+\sigma_{\rm g}^2)}{2\pi G(\Sigma_\star+\Sigma_{\rm g})} \left(= \frac{KQ_\star}{2}\frac{1+s^2}{1+\frac{s}{q}} \right), \tag{3.14}$$

and $\mathcal{K}_{\rm min}$, the $\mathcal{K}$ that minimizes $\omega^2(k)$, is found analytically by Elmegreen. The analytical expression for $\mathcal{K}_{\rm min}$ returns the correct value as long as $\omega^2(k)$ only has one minimum, but when there are two minima present it will not always return the smallest one. From Sect. 3.2 we know that inside the two-phase region of Bertin & Romeo (1988) there are two minima. This entirely analytical expression can thus only be trusted outside the two-phase region, or when we know that the smallest minimum is found.

As $Q_{\rm Elm}$ is a purely analytical parameter, the stability thresholds of Elmegreen are faster to compute than the other fluid-fluid stability thresholds, in which a minimum or maximum must be found numerically. The drawback is of course that it is not valid in the whole s-q plane.

In the lower left panel of Fig. 3.13, we show the contours of the stability threshold calculated from this effective stability parameter. Besides the region where we know that the effective stability parameter is valid, we have also included the results from inside the two-phase region. We see that the contours of the stability threshold found from Elmegreen (1995) agree with those found from Eq. (3.1) everywhere except in the stellar phase of the two-phase region.

3.5.4 Jog (1996)

The last comparison is made with the stability thresholds computed from Jog (1996). She defines the effective stability parameter as

$$\frac{1}{1+(Q_{\mathrm{Jog}})^2} = \frac{1-\epsilon}{l_{\mathrm{s-g}}\{1+[Q_\star^2(1-\epsilon)^2]/(l_{\mathrm{s-g}}^2 4)\}} + \frac{\epsilon}{l_{\mathrm{s-g}}[1+Q_{\mathrm{g}}^2\epsilon^2/(l_{\mathrm{s-g}}^2 4)]}, \tag{3.15}$$

where ϵ is given by

$$\epsilon = \frac{\Sigma_{\mathrm{g}}}{\Sigma_\star + \Sigma_{\mathrm{g}}} \left(= \frac{1}{1+\frac{q}{s}}\right), \tag{3.16}$$

and $l_{\mathrm{s-g}}$ is the dimensionless least stable wavelength, a quantity that has to be found numerically by minimizing the dispersion relation.

As this effective stability parameter cannot be written on the simple form $Q_{\mathrm{Jog}} = Q_\star/\overline{Q}$ we have to find the stability threshold by numerically computing the value of $Q_\star$ at which the disc is marginally stable. The contours of this threshold are shown in the lower right panel of Fig. 3.13, where we see that they coincide with the ones of Rafikov's fluid-fluid case.

4

Conclusions

In this thesis, we have compared two instability criteria, introduced by Rafikov (2001), for two-component galactic discs consisting of stars and gas. The first of these criteria is based on a fluid-fluid approximation, where both stars and gas are treated as fluids, while the other one is based on a more realistic kinetic-fluid approach, where stars are treated as a collisionless component. We have analysed various stability diagnostics: the condition for star-gas decoupling, the stability threshold and the most unstable wavenumber. We have also compared the kinetic-fluid stability threshold with a simple approximation introduced by Romeo & Wiegert (2011). Finally, we have compared Rafikov's stability thresholds with those found by other authors (Lin & Shu, 1966; Bertin & Romeo, 1988; Elmegreen, 1995; Jog, 1996).

From this comparison, we draw the following main conclusions:

- The region where stars and gas decouple is slightly larger in the kinetic-fluid case than in the fluid-fluid approximation. The most affected part is the gaseous phase, i.e. where the gas dominates the onset of gravitational instability in the disc. Although the difference is not large, it can be important in places where the parameter values are close to the boundary of the region.

- The fluid-fluid approximation is able to reproduce the qualitative behaviour of the stability threshold. The relative error of the effective stability parameter is never larger than 7%. The simpler approximation by Romeo & Wiegert (2011) also works well when compared to the kinetic-fluid case: the relative error is never above 10% and it is always positive.

- Concerning the most unstable wavenumber, the fluid-fluid approximation performs well in most of the parameter plane. There is however a tight region, around the transition between the stellar and gaseous phases, where the approximation breaks down and the error gets very large.

- The fluid-fluid stability thresholds of Bertin & Romeo (1988), Elmegreen (1995) and Jog (1996) are all identical to those of Rafikov. The same is true for the kinetic-fluid stability threshold of Lin & Shu (1966).

Possible future work includes the extension of the approximation proposed by Romeo & Wiegert (2011) to include N-component discs, as well as application to data of nearby galaxies.

References

Bertin G., Romeo A. B., 1988, A&A, 195, 105

Binney J., Tremaine S., 2008, Galactic Dynamics. Princeton University Press, Princeton, NJ

Cowie L. L., Hu E. M., Songaila A., 1995, AJ, 110, 1576

Daddi E. et al., 2010, ApJ, 713, 686

Daddi E., Dannerbauer H., Elbaz D., Dickinson M., Morrison G., Stern D., Ravindranath S., 2008, ApJ, 673, L21

Elmegreen B. G., 1995, MNRAS, 275, 944

Elmegreen B. G., 1999, in Star Formation, Nakamoto T., ed., pp. 3–5

Elmegreen B. G., Elmegreen D. M., 2005, ApJ, 627, 632

Elmegreen D. M., Elmegreen B. G., Hirst A. C., 2004, ApJ, 604, L21

Förster Schreiber N. M. et al., 2009, ApJ, 706, 1364

Genzel R. et al., 2011, ApJ, 733, 101

Gil de Paz A. et al., 2007, ApJS, 173, 185

Jog C. J., 1996, MNRAS, 278, 209

Jog C. J., Solomon P. M., 1984, ApJ, 276, 114

Kennicutt R. C., 1989, ApJ, 344, 685

Kennicutt, Jr. R. C. et al., 2003, PASP, 115, 928

Leroy A. K. et al., 2009, AJ, 137, 4670

Leroy A. K., Walter F., Brinks E., Bigiel F., de Blok W. J. G., Madore B., Thornley M. D., 2008, AJ, 136, 2782

Lin C. C., Shu F. H., 1966, Proc. Natl. Acad. Sci. USA, 55, 229

Lin C. C., Yuan C., Shu F. H., 1969, ApJ, 155, 721

McKee C. F., Ostriker E. C., 2007, ARA&A, 45, 565

Rafikov R. R., 2001, MNRAS, 323, 445

Romeo A. B., Wiegert J., 2011, MNRAS, 416, 1191

Safronov V. S., 1960, Annales d'Astrophysique, 23, 979

Tacconi L. J. et al., 2010, Nature, 463, 781

Tacconi L. J. et al., 2008, ApJ, 680, 246

Toomre A., 1964, ApJ, 139, 1217

Walter F., Brinks E., de Blok W. J. G., Bigiel F., Kennicutt R. C., Thornley M. D., Leroy A., 2008, AJ, 136, 2563